Geophys. J. Int. (1996) **125,** 679–695

Shear-wave velocity models from Rayleigh-wave dispersion in the broader Aegean area

Ioannis S. Kalogeras[1] and Paul W. Burton[2]

[1] *National Observatory of Athens, Seismological Institute, PO Box* 20048, 11810 *Athens, Greece*

[2] *University of East Anglia, School of Environmental Sciences, Norwich* NR4 7TJ

Accepted 1996 January 8. Received 1995 December 28; in original form 1994 July 25

SUMMARY

An analysis of Rayleigh waves generated by earthquakes in the broader Aegean is undertaken to estimate variations in the shear-wave velocity structure in the crust and upper mantle down to about 70 km depth. The study centres literally on the vertical-component long-period standard seismograph at Athens (ATH), and is only possible because this station has provided good-quality data over many years of continuous operation. Rayleigh waves from 81 earthquakes during 1963–87, with surface-wave magnitudes in the range 4.2 to 5.4 and epicentral distances of 300–500 km from Athens are analysed. These earthquake epicentres are selected in clusters defining 12 propagation paths across the broader Aegean and radial to Athens. The highest concentration of azimuthal sampling traverses the Hellenic Volcanic Arc. The ensuing group-velocity curves over these radial paths are inverted to shear-wave velocity–depth models using linear and then Monte Carlo Hedgehog inversion schemes. The resulting velocity–depth solutions from both schemes, presented as individual path velocity–depth profiles, 3-D azimuthal perspectives and contoured velocity–depth panoramas over the whole broader Aegean, are corroborative. The western arc of azimuths extending from Chalkidiki, north of Athens, to SW Crete, south of Athens, have velocity–depth profiles which consistently reach sub-Moho velocities at about 45 km depth. The most striking feature revealed by the contoured shear-wave velocity–depth panoramas is an extensive zone of relatively low velocity, about 3.8 km s^{-1}, centred around 30 km depth, which may extend from 20 to 40 km depth. This low-velocity zone is contained in the wedge of paths from Carpathos, Rhodes and SW Turkey which traverse the Hellenic Volcanic Arc and subtend an angle of about 33° at Athens. There is also slight evidence for anomalously low velocities at greater depths (around 4.1–4.2 km s^{-1} at about 50–60 km depth) but these are at the limits of useful resolution of the available data; nevertheless, these indications are at their strongest in the same wedge below the Hellenic Volcanic Arc.

Key words: Aegean, crust, Greece, low-velocity zone, Rayleigh waves, upper mantle.

1 INTRODUCTION

Seismic surface waves generated by earthquakes or explosions show dispersion along the propagation path: the group velocity varies as a function of frequency. This variation depends on the 2-D properties of the path traversed, and the Rayleigh wave reveals average properties. The estimation of the relationship between group velocity and frequency is of great importance because from this relationship the determination of the variations of the body-wave velocity as a function of depth along the propagation path is possible. The structure of the broader area of the Aegean and the eastern Mediterranean has been investigated by several authors using various methods and techniques, for example Papazachos, Polatau & Mandalos (1966), Makris (1975, 1978), Papazachos & Comninakis (1978), Le Pichon & Angelier (1979), Panagiotopoulos (1984) and Hashida, Stavrakakis & Shimazaki (1988). Deep structure associated with subduction below the Hellenic Arc has been investigated tomographically by Spakman, Worter & Viaar (1988), and a detailed tomography below the broader Aegean has been presented by Ligdas, Main & Adams (1990).

The conclusions obtained by studies based specifically on surface waves can be summarized as follows: Papazachos, Polatou & Mandalos (1967) and Papazachos (1969) concluded that the mean thickness of the crust of the area varies between 35 and 45 km; Payo (1967, 1969) characterized the Aegean as an area of continental crust that is covered by a rather thick sedimentary layer; Calcagnile *et al.* (1982) proposed further

© 1996 RAS

research to determine the existence of a crust–mantle transition zone in the Aegean, a feature which they accepted in other areas of the eastern Mediterranean; Ezen (1988, 1991a,b) studied the effect of crustal thickness on Rayleigh-wave records and proposed a *P*-wave velocity model for western Turkey; and Kalogeras, Drakopoulos & Burton (1993) determined the mean dispersion curve for a Dodecanese to Athens propagation path and concluded that the predominantly continental structure of the SE Aegean shows, at its deepest parts, a possible contamination by oceanic material.

Recent studies on geodynamic processes in the Aegean area (e.g. Makropoulos & Burton 1984; Ligdas, Main & Adams 1990; Christova & Nicolova 1993; Hatzfeld *et al.* 1993) show that the Hellenic Arc and the adjacent areas are tectonically more complicated than had previously been thought. It should be emphasized that there is no generally accepted single geotectonic model that gives an explanation for all of the geological and geophysical observations in the Aegean, and improved knowledge of seismological parameters or structural models will help discriminate between different geotectonic and rheological models. The purpose of this study is therefore to apply inversion techniques to the dispersion of Rayleigh waves along various representative propagation paths covering the broader area of the Aegean, in order to obtain a shear-wave velocity structure of this whole area.

2 DATA, ANALYSIS AND PRELIMINARY DISCUSSION

The Rayleigh-wave records used in this study were generated by 81 earthquakes which occurred in the broader Aegean area during 1963–87 inclusive, with epicentral distances between 300 and 500 km from Athens and surface-wave magnitudes between 4.2 and 5.4 M_s. The earthquakes were all recorded by the vertical component of the Worldwide Standard Seismograph Network (WWSSN) long-period seismograph of the National Observatory of Athens (ATH). Although Greece is the country with the highest seismicity in Europe, it is continuity of station operation that has provided the opportunity to collect a homogeneous data set from one instrument spanning 25 years of observation. Table 1 is a listing of the

Table 1. Epicentral parameters of the earthquakes used in this study (source: ISC bulletins).

Date	Origin time	Location Lat. N°	Location Lon. E°	Focal Depth km	Epic. Dist. d°	Magn. M_s
1963/01/31	15 07 04.0	35.92	21.86	60	2.53	5.1
1965/08/24	23 57 35.4	40.39	26.20	18	3.09	4.2
1965/08/25	04 57 45.7	34.72	25.08	10	3.43	4.8
1966/08/16	03 53 41.7	40.16	19.75	20	3.78	4.9
1967/05/15	08 12 58.0	34.53	26.64	35	4.17	4.9
1967/09/06	04 59 23.0	35.06	23.09	20	2.95	4.8
1968/05/30	17 40 26.1	35.45	27.88	27	4.19	5.3
1968/06/12	09 05 04.0	35.30	27.89	16	4.29	4.6
1968/07/08	17 41 06.4	34.47	25.08	38	3.66	5.3
1968/07/27	02 45 51.0	35.43	27.92	29	4.23	5.0
1968/09/28	00 53 28.0	40.49	26.38	28	3.26	4.4
1969/03/24	01 59 34.0	39.11	28.51	30	3.93	5.0
1969/03/25	14 18 52.1	39.17	28.49	34	3.93	4.8
1969/03/28	10 02 17.4	39.13	28.45	37	3.89	4.9
1969/04/16	04 54 12.8	35.30	27.90	55	4.30	4.8
1969/04/16	22 55 40.5	35.32	27.77	52	4.20	5.1
1969/04/17	00 54 38.2	35.19	27.83	55	4.32	4.8
1969/04/30	20 20 32.0	39.10	28.50	08	3.93	5.0
1969/05/01	18 02 16.4	35.41	27.68	51	4.08	5.1
1969/05/01	20 06 45.4	35.39	27.73	67	4.13	4.7
1969/05/14	10 05 17.1	35.33	27.72	43	4.16	5.1
1969/05/15	12 05 57.0	35.30	27.70	46	4.20	4.8
1969/06/14	13 47 26.4	34.34	25.05	21	3.78	5.0
1969/09/28	22 54 08.0	34.30	25.15	29	3.84	5.3
1969/10/07	05 09 12.0	39.20	28.40	13	3.87	4.9
1970/04/23	09 01 26.6	39.13	28.65	28	4.04	5.2
1970/11/11	20 58 12.0	36.00	28.20	35	4.12	4.9
1971/01/03	23 18 43.0	34.63	26.32	47	3.94	5.1
1971/07/03	04 05 55.4	35.15	27.89	40	4.39	4.5
1972/09/16	03 53 26.4	40.28	19.73	15	3.86	5.0
1973/01/26	07 50 11.0	35.74	22.08	41	2.59	4.8
1973/04/06	14 13 57.3	34.41	25.18	37	3.75	5.1
1973/10/14	18 07 06.0	34.68	26.31	51	3.90	4.7
1975/03/16	08 37 16.3	40.36	26.14	05	3.04	4.3
1975/03/17	02 06 39.1	40.48	26.03	02	3.08	4.5
1975/03/27	19 42 42.5	40.48	26.08	05	3.11	4.5
1975/11/12	09 03 49.0	36.28	28.15	64	3.92	5.3
1975/11/22	10 06 08.4	39.92	20.11	34	3.42	5.1
1976/06/25	07 01 06.6	35.07	23.25	22	2.92	5.0
1977/09/10	06 31 42.0	34.93	23.09	24	3.08	4.9
1977/09/12	02 57 55.0	34.91	23.23	38	3.08	4.9
1977/09/14	18 49 05.0	34.86	23.07	19	3.15	5.0
1977/10/22	10 02 08.3	34.90	23.16	28	3.10	5.1
1978/01/12	20 08 37.6	35.83	22.27	59	2.43	4.6
1978/03/07	22 33 46.6	34.48	25.24	41	3.69	5.4
1978/05/24	02 12 28.1	40.71	23.34	08	2.75	4.8
1978/06/19	10 31 05.5	40.77	23.24	10	2.82	5.3
1978/06/21	12 29 43.1	40.81	23.06	01	2.88	4.8
1978/07/04	22 23 28.4	40.75	23.06	18	2.82	5.0
1980/10/04	15 12 06.6	37.00	28.80	26	4.16	5.0
1981/01/22	16 25 44.9	34.16	25.25	49	4.00	4.7
1981/06/24	18 41 27.6	37.85	20.13	22	2.84	5.1
1981/06/24	22 52 11.5	37.81	20.06	20	2.90	4.8
1981/06/29	08 48 16.0	37.78	20.00	11	2.94	4.8
1981/07/03	02 32 28.5	37.91	19.97	16	2.96	4.8
1981/07/12	17 14 40.2	37.88	20.06	23	2.90	4.8
1981/07/17	06 30 55.8	34.88	22.85	19	3.17	5.1
1981/09/14	01 21 38.8	34.73	25.05	26	3.41	4.9
1983/01/18	22 34 40.0	38.05	20.09	09	2.86	4.6
1983/01/19	05 41 50.0	37.85	19.95	28	2.98	5.3
1983/03/24	12 50 58.2	38.15	20.23	17	2.76	4.9
1983/03/24	19 35 55.3	38.22	20.11	19	2.86	4.8
1983/11/08	18 21 26.6	37.88	20.13	39	2.84	4.9
1983/11/25	12 19 23.6	34.95	22.80	25	3.11	5.0
1984/02/05	00 20 19.7	37.21	28.67	30	4.01	5.0
1984/02/19	03 47 22.5	40.67	23.36	24	2.70	4.9
1984/04/21	07 33 33.0	35.85	21.77	42	2.64	5.1
1984/06/16	16 21 32.9	35.03	22.89	42	3.01	4.9
1984/07/02	07 48 49.0	34.95	22.98	38	3.08	4.8
1984/07/03	18 08 10.7	34.95	22.94	44	3.08	4.8
1984/07/15	12 34 33.8	34.89	22.91	40	3.15	4.6
1984/07/29	01 58 43.3	40.45	25.91	21	3.00	5.0
1984/07/29	09 48 23.8	40.43	25.93	27	2.99	4.5
1985/04/07	13 33 45.7	37.89	20.04	27	2.91	4.9
1985/04/21	08 49 40.0	35.66	22.17	35	2.62	5.1
1986/04/27	09 27 06.0	34.73	23.33	27	3.25	5.0
1986/05/22	19 52 22.0	34.64	26.52	48	4.02	5.2
1987/02/13	13 58 06.2	40.22	19.87	00	3.74	4.5
1987/10/05	09 27 02.0	36.24	28.27	27	4.03	5.1
1987/10/25	13 02 00.0	36.30	28.35	24	4.07	4.6
1987/12/10	05 44 30.0	34.84	26.73	07	3.97	4.8

focal parameters of these earthquakes. The earthquakes were grouped or clustered so that they represent different propagation paths to the recording station of ATH. The map of Fig. 1 illustrates the individual epicentres and clusters of the earthquakes used and the propagation paths. Azimuthal sampling in Fig. 1 will be discussed later.

The seismograms were digitized manually at unequal time intervals and subsequently interpolated to obtain an equal time interval of 0.5 s. This determines a Nyquist frequency of $f_N = 1$ Hz, although in practice only frequencies lower than 0.13 Hz with adequate spectral signal-to-noise ratio were of interest.

The signals were analysed to obtain the group velocity using the multiple-filter technique of Dziewonski, Bloch & Landisman (1969), as modified by Burton & Blamey (1972). The digitized signals were transformed into the frequency domain using the Fast Fourier Transform algorithm of Cooley & Tukey (1965) and the spectra obtained were then corrected for the WWSSN instrument response using the Espinosa, Sutton & Miller (1965) technique—measurements were taken from the seismogram calibration pulse and hence the parameters of the instrument were estimated. This allows for any slight temporal variation in the parameters of the long-period vertical-component WWSSN instrument at Athens. The filters then used to determine instantaneous spectral amplitudes, and hence group velocity at each frequency, were of constant resolution. We obtain 15 independent values of group velocity at fixed frequencies in the range 0.02–0.13 Hz approximately.

The group velocities are estimated for the same set of Fourier harmonics for all the seismograms, and the dispersion data are averaged over the cluster of earthquakes for each propagation path. Fig. 2 shows the mean dispersion curves for the 12 propagation paths. The estimated group-velocity values have been presented with 99.5 per cent confidence intervals. These dispersion curves show that the propagation paths are characterized by different types of behaviour, especially for the range of lower frequencies, which correspond to penetration into deeper parts of the lithosphere (about 40–70 km). The lower or higher group velocities, for the range of higher frequencies, are influenced by the existence of a thicker or thinner top sedimentary layer respectively.

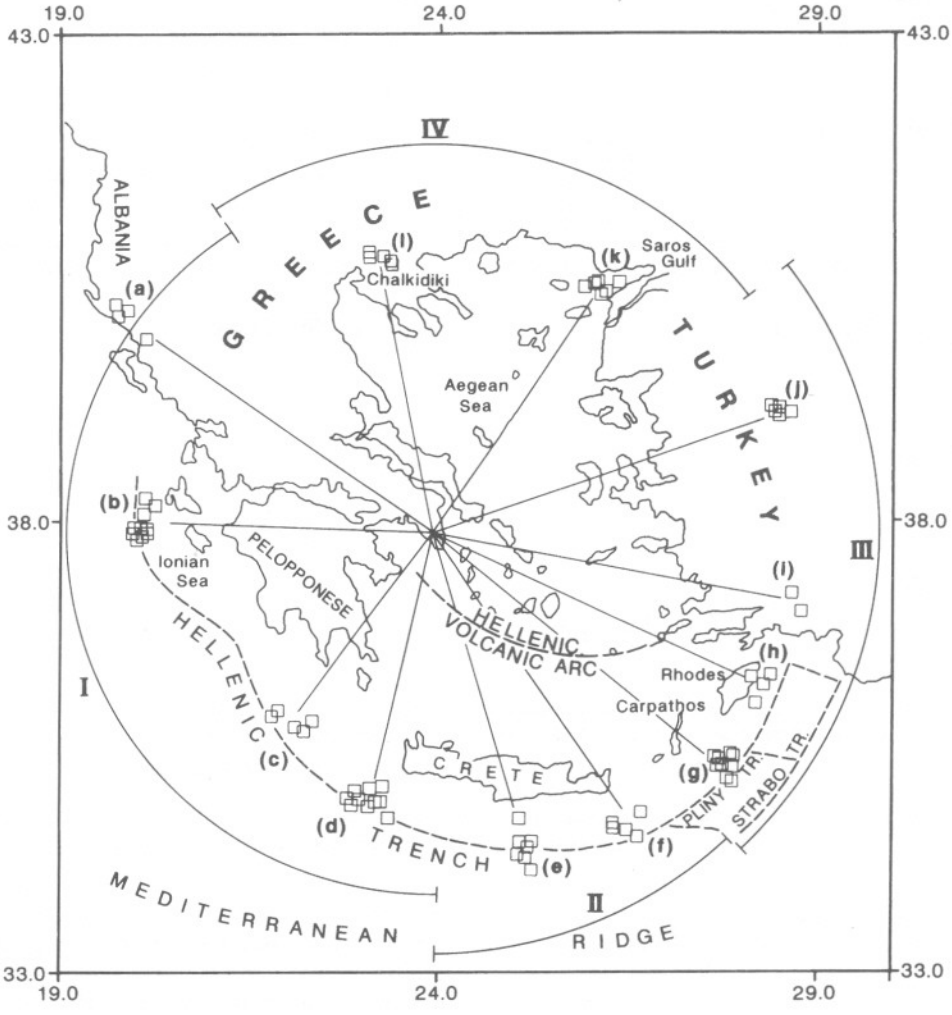

Figure 1. Epicentres and clusters of earthquakes and the Rayleigh-wave propagation paths a–l used in this study. Listed in a counter-clockwise direction, these propagation paths to Athens are from: (a) Greek–Albanian border, (b) Ionian sea, (c) SW Peloponnese, (d) SW Crete, (e) Crete, (f) SE Crete, (g) Carpathos, (h) Rhodes, (i) SW Turkey, (j) central western Turkey, (k) Saros Gulf and (l) Chalkidiki. The arcs labelled I–IV bracket propagation paths over which the Rayleigh-wave dispersion characteristics are similar and wedges of lithosphere beneath which the inversions to velocity–depth models also show similarities (discussed in the text). The angles these wedges subtend at Athens can be measured opposite the arcs labelled I–IV.

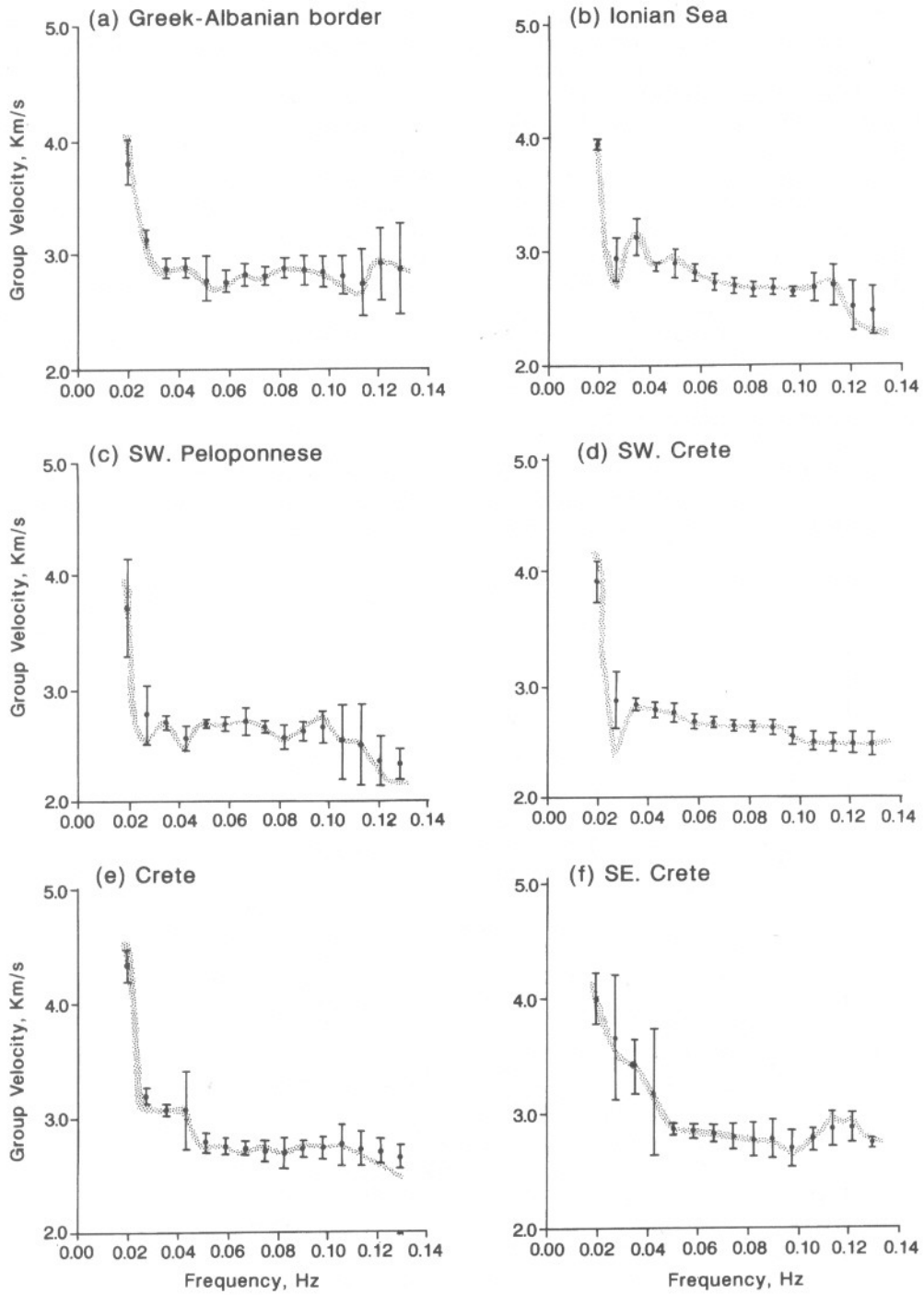

Figure 2. Mean dispersion curves of the Rayleigh waves along the 12 propagation paths a-l, plotted with 99.5 per cent confidence intervals. The superimposed shaded areas represent the forward solutions obtained from the ensuing linear inversion models illustrated in Fig. 4.

Some of the individual dispersion curves of Fig. 2 have certain characteristics in common, and they can, by inspection, be divided into four broad groups.

Group I: Greek–Albanian border, Ionian sea, SW Peloponnese and SW Crete (a–d of Fig. 2). These four dispersion curves all show one high value of group velocity in the range 3.7–3.9 km s^{-1} at the lowest frequency (0.02 Hz), while all other group velocities are with few exceptions less than 3.00 km s^{-1} throughout the spectrum. With the exception of the lowest frequency these curves show little character (such as turning points, inflections, or changes of gradient).

Group II: Crete and SE Crete (e–f of Fig. 2). These two dispersion curves show a very high value of group velocity in the range 4.0–4.35 km s^{-1} at the lowest frequency and a steady increase in velocity to this maximum from below 0.051 Hz. All group velocities from 0.051 Hz upwards are less than 3.0 km s^{-1}, where the curve is approximately flat.

Group III: Carpathos, Rhodes, SW Turkey and central western Turkey (g–j of Fig. 2). These four dispersion curves all

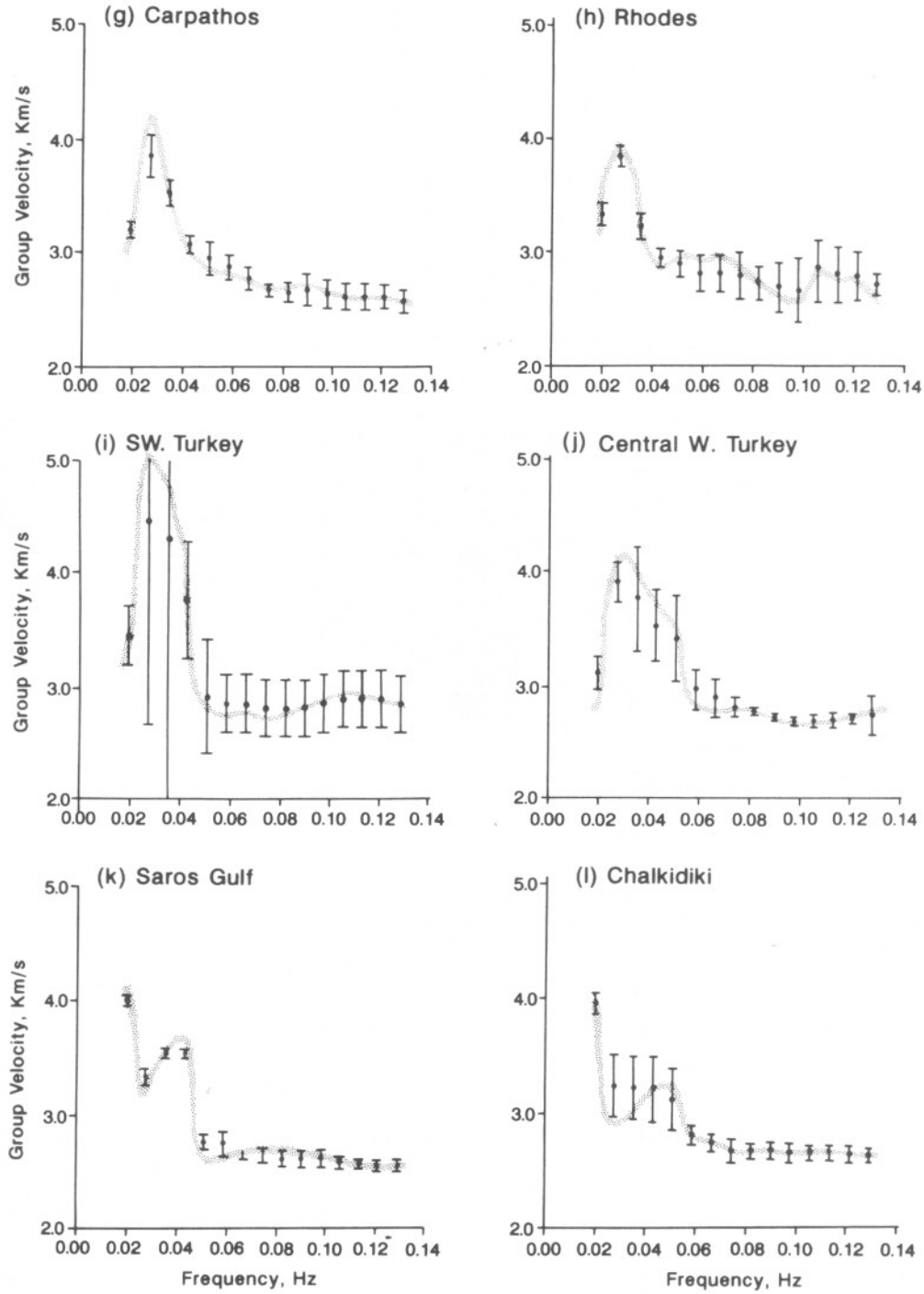

Figure 2. (*Continued.*)

show a turning point or roll-over in the group-velocity curve with a maximum at 0.027 Hz. *This is an extremely important characteristic.* This peak is systematically at 3.85–3.9 km s^{-1} (excluding SW Turkey to Athens, which displays a poor confidence interval on velocity at the frequency of the turning point; see i in Fig. 2) and forms within the low frequency range from 0.051 Hz.

Group IV: Saros Gulf and Chalkidiki (k–l of Fig. 2). These two dispersion curves show a high value of group velocity, in the range 3.95–4.0 km s^{-1} at the lowest frequency, and an increase towards this velocity through frequencies below about 0.051 Hz. Velocities at higher frequencies are less than 3.0 km s^{-1}. The Saros Gulf path (k in Fig. 2) is also unusual in that it reveals a well-constrained sub-peak within 0.035–0.043 Hz (which subsequently proves difficult to model).

Fig. 3 provides a schematic and thought-provoking representation of the data drawn from Fig. 2, which needs to be interpreted with care. For each propagation path seven values of group velocity are extracted for the same set of frequencies and related to an effective penetration depth or skin depth according to the relation of Knopoff (1972). This connects the penetration

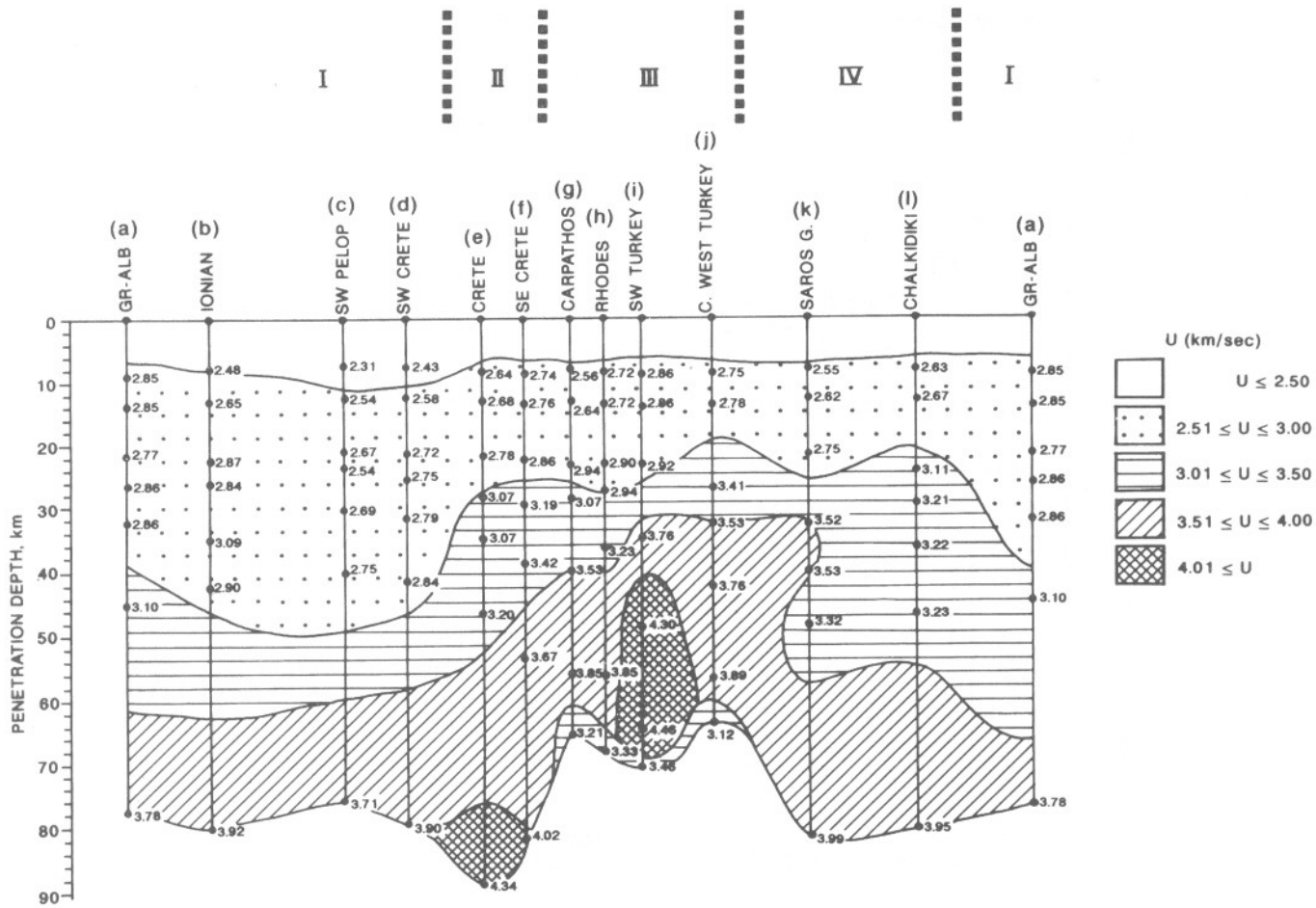

Figure 3. Schematic synthesis of Rayleigh-wave penetration depths based on the dispersion data of Fig. 2. Seven values of group velocity are extracted for the same set of frequencies for each propagation path in relation to penetration depths obtained from Knopoff's (1972) relation. The length a–a represents 360°, and spacings between radial propagation paths are proportional to the angle subtended at Athens between two great-circle paths. Groups I–IV each encompass dispersion curves with common characteristics.

depth pd (km) with the wavelength λ (km), and thus with the group velocity U (km s^{-1}) and the frequency f (Hz):

$$pd \approx 0.4\lambda = 0.4U/f.$$

The frequencies chosen are 0.020, 0.027, 0.035, 0.043, 0.051, 0.082 and 0.130 Hz. The propagation paths that represent the south-west of the study area are paths of relatively lower group velocities, while the paths that represent the south-east show a complicated character for penetration into the structure of the upper mantle. The general shape shown in Fig. 3 is similar to the description provided by Makris (1978), in which the area of the central Aegean is characterized by a large dome of hot asthenospheric material ascending into the lithosphere, causing expansion and crustal thinning, while elsewhere the thick crust of the western Hellenides is apparent. Quite clearly, scaling the penetration depth to 0.5λ or 0.6λ, $0.5U/f$ or $0.6U/f$, would scale the depth represented to greater depth without changing the shape in Fig. 3.

The four Groups I–IV summarizing the major characteristics of the dispersion curves of Fig. 2 carry through into Fig. 3 and are marked on it. These characteristics clearly separate into distinct wedges of azimuth. Group I suggests a wide azimuth wedge to the west with a relatively simple and deep penetrating structure possessing a thick lid; Group II, with a more rapid onset of higher-velocity at lower frequencies, suggests a shallower penetration to higher-velocity material and a transition to the complications of Group III; Group III suggests a thinner-lidded structure with higher-velocity material surmounting a possible low-velocity zone at depth; Group IV represents a transitional wedge back to the simpler Group I structure, passing through the Saros Gulf azimuth which contains anomalies differing slightly from Group III but lacking the low velocity at the lowest frequency.

It should be noted that Fig. 3 is azimuthally accurate, i.e. a–a represents 360° and the spans between propagation paths are proportional to the angle subtended at Athens. The arcs drawn in Fig. 1 to represent Groups I–IV are in accord with the divisions indicated in Fig. 3, and the angles subtended at Athens by these arcs correspond to the wedges of lithosphere sampled by Groups I–IV. The angle subtended at Athens by the structurally complicated wedge between the Carpathos and the central western Turkey propagation paths is about 57°; the overall wedge nominally subtended by Group III is about 85°. The azimuthal resolution in Fig. 3 is not accidental. The Carpathos to Athens propagation path was the first examined in this study and, as a result of the complexity it revealed, nearby azimuths of SE Crete and Rhodes to Athens were selected. This philosophy resulted in a relatively denser sam-

pling of the complications in the SE of the broader Aegean than elsewhere.

3 INVERSION OF GROUP-VELOCITY DATA

The average dispersion curves and related uncertainties are used to estimate the average distribution of the shear-wave velocity with depth along each propagation path. For this reason the dispersion curves are directly inverted using two well-established but different approaches: a linearized inversion scheme (Backus & Gilbert 1967, 1968, 1970; Wiggins 1972) and the Hedgehog modification of the Monte Carlo inversion (Keilis-Borok & Yanovskaja 1967; Valus 1968). These schemes for Rayleigh-wave dispersion inversion are highly appropriate for non-intersecting great-circle propagation paths where lithospheric blocks are not traversed by multisource, multi-directional ray paths. Each inversion scheme requires a model of shear-wave velocity variation versus depth as a starting model in order to calculate initial theoretical dispersion curves which are to be compared to those observed; the starting model is then perturbed to improve the goodness-of-fit of the model to data. The starting models used in this study are modifications of models proposed by previous investigators for parts, or for the whole, of the area. A mean starting model used uniformly throughout the broader Aegean only produces results or inverse models in some areas, not in others. The starting models listed in Table 2 are modified slightly from those of the authors referenced with respect to velocity and, importantly, with respect to layer thickness. The modifications are systematic. Where layers have been combined, shear-wave slownesses have been averaged, weighted for layer thickness.

Table 2. The modified published models used as final starting models for the inversion schemes. Shear-wave velocity β (km s^{-1}) is given as a function of depth and layer thickness d (km) for each of the propagation paths a–l.

Propagation path: *a* Greek-Albanian border; *c* SW Peloponnese; *d* SW Crete; *f* SE Crete
Reference: Panagiotopoulos, 1984

d (km)	β (km/s)
12.0	3.25
15.0	3.47
16.0	3.82
17.0	4.57
	4.57

Propagation path: *b* Ionian sea
Reference: Panagiotopoulos, 1984

d (km)	β (km/s)
12.0	3.25
15.0	3.47
16.0	3.82
	4.57

Propagation path: *e* Crete
Reference: Panagiotopoulos, 1984

d (km)	β (km/s)
18.0	3.41
12.0	3.82
30.0	4.57
	4.57

Propagation path: *g* Carpathos; *h* Rhodes
Reference: Makris, 1977

d (km)	β (km/s)
10.0	2.66
10.0	3.40
11.0	3.62
29.0	4.38
	4.38

Propagation path: *i* SW Turkey
Reference: Papazachos *et al.*, 1966

d (km)	β (km/s)
16.0	3.19
15.0	3.48
11.0	3.98
18.0	4.55
	4.55

Propagation path: *j* Central western Turkey; *l* Chalkidiki
Reference: Panagiotopoulos, 1984

d (km)	β (km/s)
7.0	3.33
12.0	3.48
12.0	3.82
29.0	4.57
	4.57

Propagation path: *k* Saros Gulf
Reference: Papazachos *et al.*, 1967

d (km)	β (km/s)
7.0	2.85
15.0	3.60
15.0	4.00
23.0	4.50
	4.50

This is particularly the case for relatively thin layers; these have usually been combined into a thicker layer. The half-space layer was imposed at 60 km, allowing some penetration expected from the longer-wavelength Rayleigh waves which nominally penetrate to about a 70 km skin depth for these data sets. The final starting model selected for each of the 12 propagation paths was that which gave the best χ^2 during the linear inversion scheme. Table 2 summarizes the final starting models and their related references. Theoretical dispersion curves are calculated from these starting models using the Schwab & Knopoff (1972) algorithm and the Thompson–Haskell matrix method. In this algorithm, the Poisson ratio is set equal to 0.25, corresponding to the relation $\alpha = \sqrt{3}\beta$ between the *P*-wave and the shear-wave velocities. Keller *et al.*'s (1976) relation between density and shear-wave velocity is also used throughout. These identities reduce the number of inversion parameters and the results are not sensitive to these choices. The formal inversion schemes referenced above are well known and therefore only a broad outline of the two schemes will be given below.

To allow a linear inversion scheme, the relation between the model parameters and dispersion curve has to be linearized. The algorithm requires a matrix of partial derivatives, connecting variations of the group slowness with small variations or perturbations in the parameters (shear-wave velocities) of the earth model. Perturbations in the shear-wave velocity model are solved for iteratively until the calculation of these small variations in the earth-model parameters produces an earth model that provides a good fit to the observed dispersion data, and further iterations will provide no noticeable improvement to this goodness-of-fit. Resolution kernels are used in Fig. 4 to illustrate the quality of the solution, including the inevitable uncertainty of the solution, particularly in the deeper layers. The goodness-of-fit of the forward solution to the observed dispersion data is illustrated in Fig. 2.

The linear inversion solutions are then used to guide the initial form of the parameter range (shear-wave velocity) within which the Hedgehog models are sought. In practice, the linear inversion solution lies at the centre of the Hedgehog search range within each layer. In the Hedgehog inversion scheme, accepted families of models are those for which the differences between the corresponding theoretical and the observational dispersion data for a set of closely linked earth models are as small as reasonably possible. These differences are expressed by two quantities, a and σ. The quantities monitored are

$$\left|\frac{U_i - U_{oi}}{\Delta U_{oi}}\right| = a$$

and

$$\sqrt{\frac{1}{M}\sum_{i=1}^{M}\left(\frac{U_i - U_{oi}}{\Delta U_{oi}}\right)^2} = \sigma,$$

where U_{oi} is the observed dispersion curve with associated uncertainties ΔU_{oi} for frequencies $i = 1 \ldots M$, and U_i is the theoretical dispersion curve derived from an N-layered model of shear-wave velocity β_l and layers $l = 1 \ldots N$. A model is accepted when these differences are less than both a and σ. The stringency of these tests can be changed by varying the values for a and σ.

Table 3 summarizes the numerical results from the inversions of the dispersion curves and Fig. 4 illustrates the shear-wave velocity profiles as a function of depth from both inversion schemes for each of the 12 propagation paths. Table 3 also summarizes the range of shear-wave velocity searched and the degree of model perturbation or resolution, $\delta\beta_l$, available in any one layer during the final Hedgehog inversion. The single-path inversion results contained in Fig. 4 are combined in Fig. 5 to provide a 3-D representation of the variations of shear-wave velocity with depth throughout the broader Aegean. In these graphs the depth scale remains constant, whereas the velocity scale varies so that the length of the great-circle propagation path corresponds to the lowest shear-wave velocity calculated for that path (actual velocity values in Table 3).

4 RESULTS

The complex structure of the crust and upper mantle of the broader Aegean becomes very apparent, particularly in the comparative azimuthal perspectives provided in Fig. 5. The use of an average model for the whole area is clearly much inferior. More specifically, considering the inversions on a path-by-path basis through Groups I–IV, and examining Figs 4 and 5 and Tables 2 and 3, we obtain the following results.

Greek–Albanian border and Ionian sea (a–b of Figs 4 and 5)

Fundamentally the same starting model was used for these two paths, except that the depth of the half-space has been introduced at a shallower depth in the linear inversion of the Ionian sea path, to obtain solutions below 43 km. The shear-wave velocity increases monotonically with depth along both paths. The velocity in the first, shallowest layer is higher for the Greek–Albanian border path than that for the Ionian sea. There is a substantial increase of the velocity into the fourth layer below 43 km for the Ionian sea path, and this is prolonged into the half-space below 60 km in the Hedgehog inversion and apparent in both inversion techniques. Sub-Moho velocities (shear-wave velocity of about 4.5 km s^{-1} or greater) are not seen until this fourth layer below 43 km.

SW Peloponnese, SW Crete, Crete and SE Crete (c–f of Figs 4 and 5)

The same starting model was used for these paths, with the exception of a modification for the Crete path to achieve an acceptable solution. The two western paths (c and d) show a significantly low velocity below 3.00 km s^{-1} in the first layer, in the linear inversion, which is substantiated by the Hedgehog solution. These two paths span the deepest water in the Aegean. Both western paths show similar overall behaviour in the variation of shear-wave velocity with depth. The significant increase of velocity with penetration into the fourth layer below 43 km is again apparent. These properties are reflected in both linear and Hedgehog inversions. However, the velocities in the shallowest layer along the two eastern paths (e and f) are very similar to each other but higher than for the two western paths; indeed, they are effectively identical to that observed for the Greek–Albanian border inversion. There are differences observed in the other layers. In particular, the onset of rapid increase in velocity is shallower in the case of the SE Crete inversion, the major increases being initiated in the third

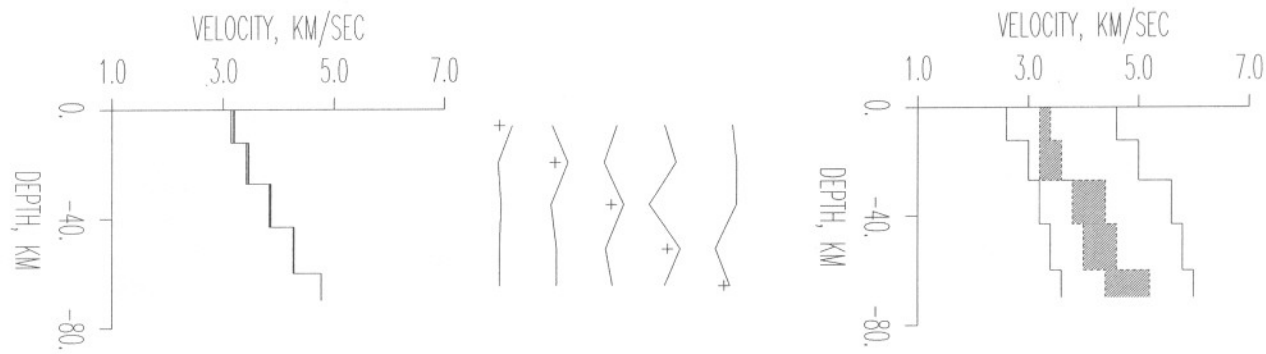

(a) : Greek–Albanian border

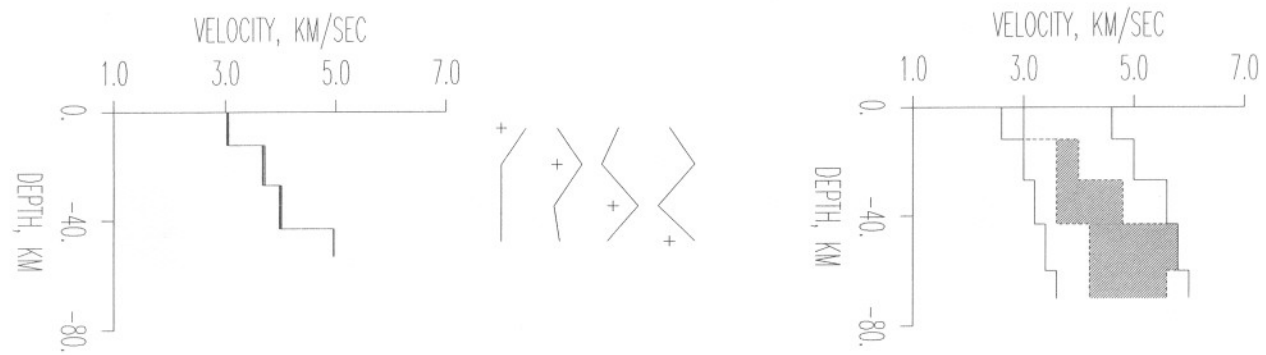

(b) : Ionian sea

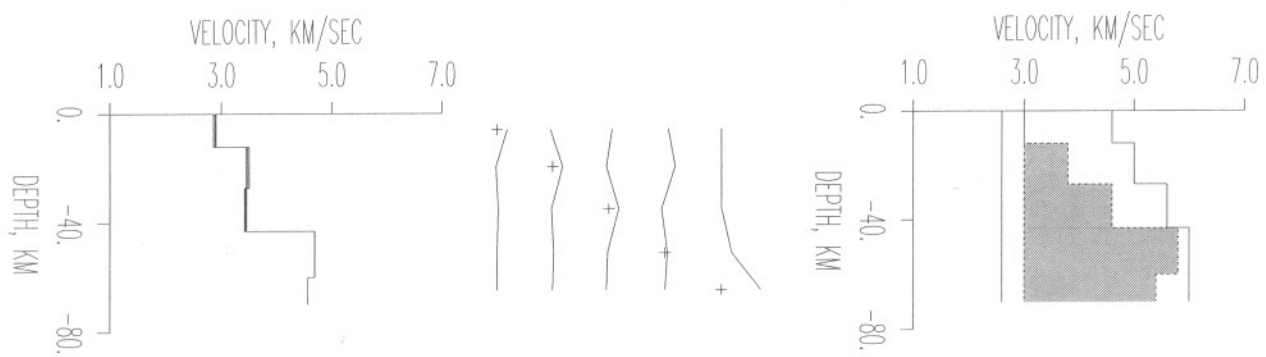

(c) : SW Peloponnese

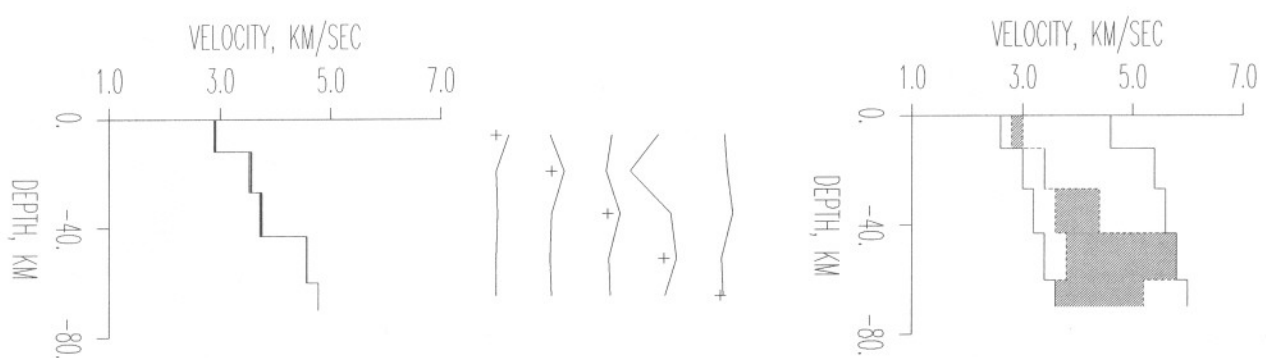

(d) : SW Crete

Figure 4. Shear-wave velocity–depth models along the radial propagation paths a–l resulting from the linear inversion (graphs on the left) and the Hedgehog technique (graphs on the right) applied to the dispersion data. Resolution kernels representing the quality of the solution of the linear inversion are also shown. For the Hedgehog technique, continuous lines border the region of search, while the dashed lines and shaded area show the region of the connected Hedgehog solutions.

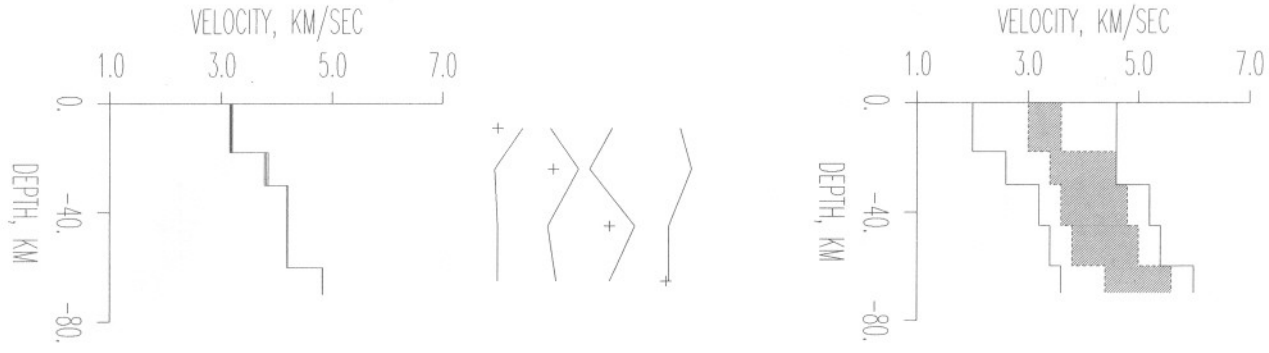

(e) : Crete

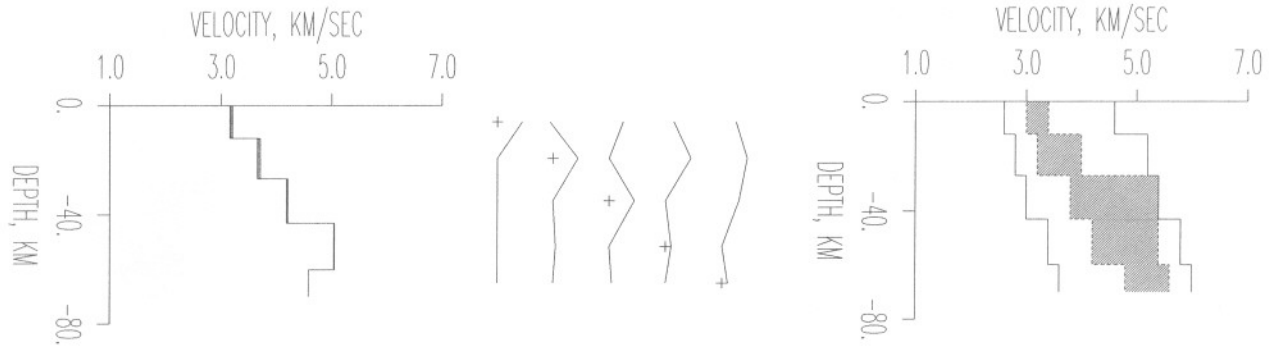

(f) : SE Crete

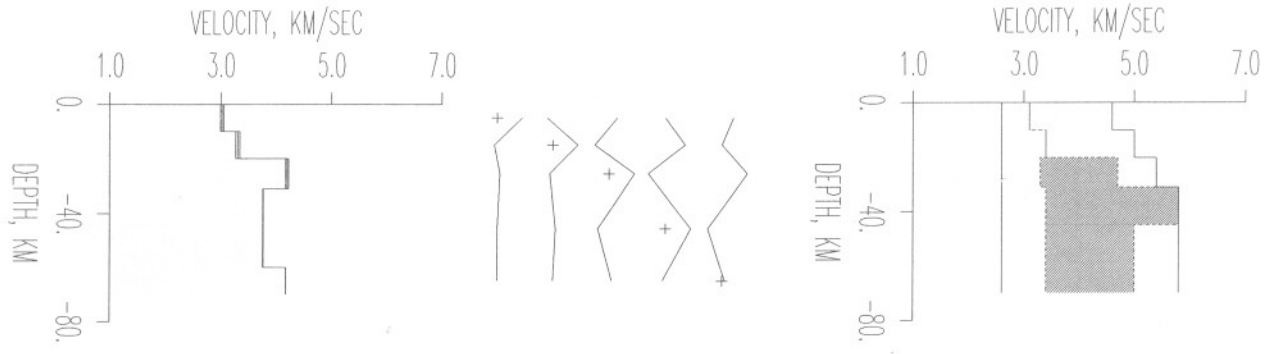

(g) : Carpathos

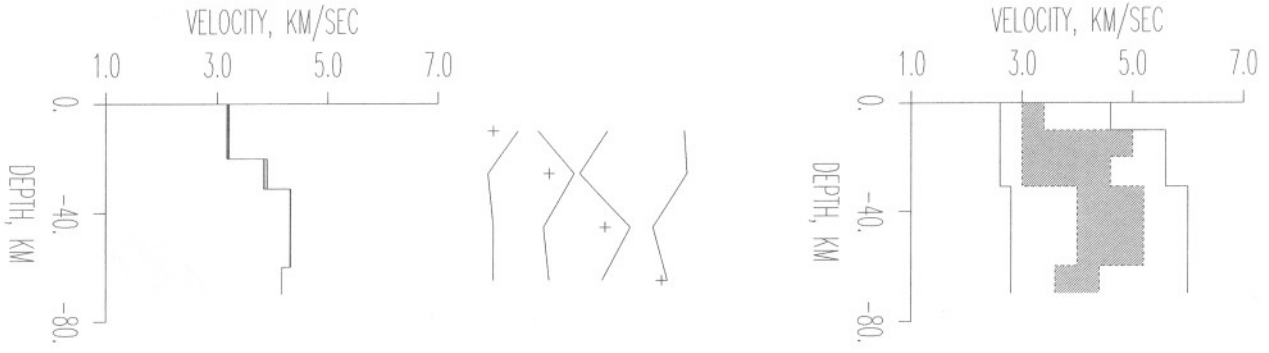

(h) : Rhodes

Figure 4. (*Continued.*)

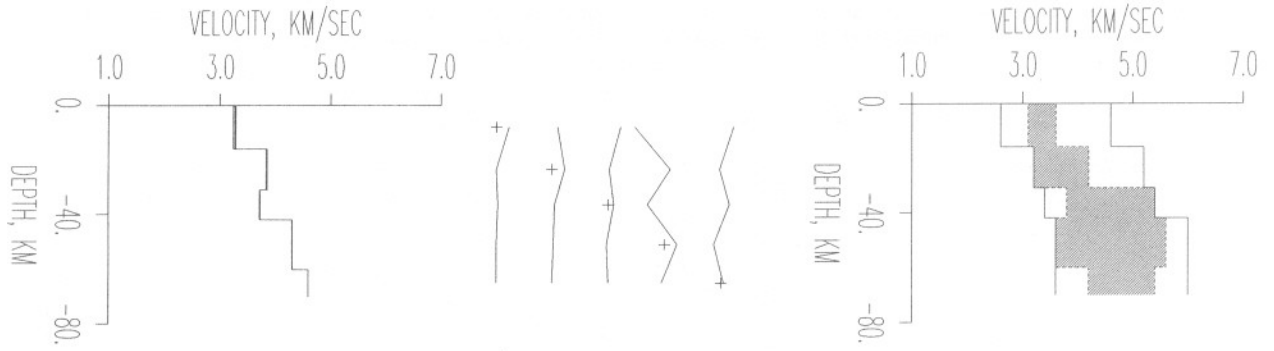

(i) : SW Turkey

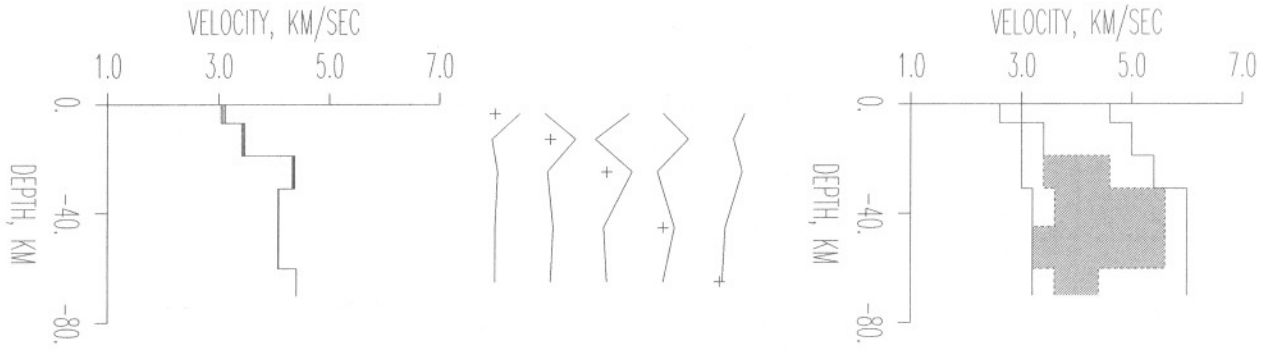

(j) : Central western Turkey

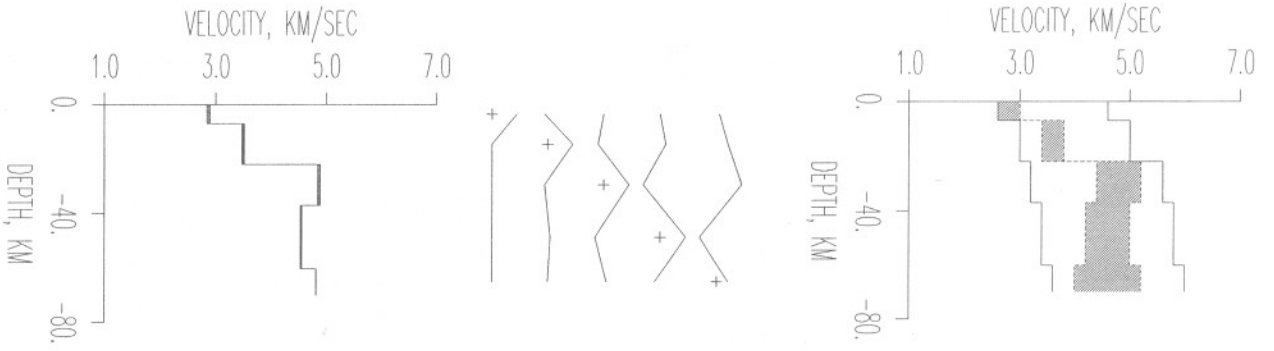

(k) : Saros gulf

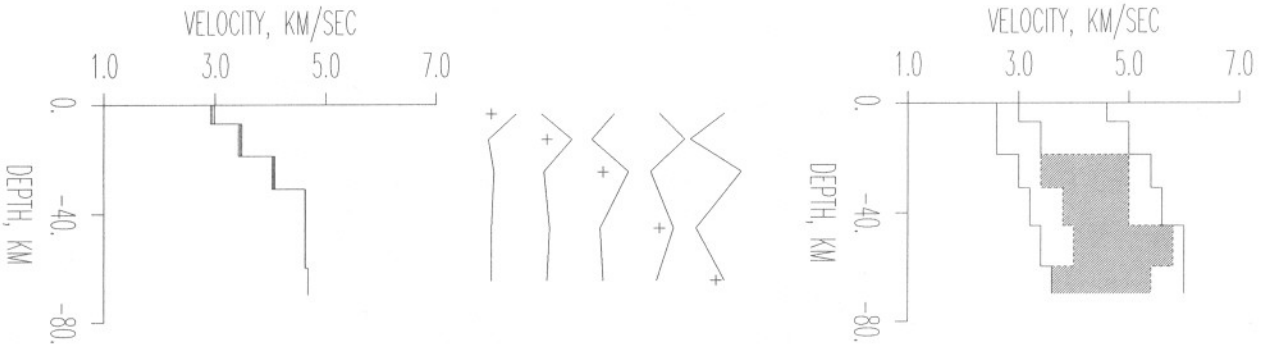

(l) : Chalkidiki

Figure 4. (*Continued.*)

Table 3. The shear-wave velocity β (km s^{-1}) as a function of depth and layer thickness d (km) for the different propagation paths a–l, resulting from the linear inversion and the Hedgehog inversion of the dispersion curves.

	LINEAR INVERSION		HEDGEHOG INVERSION			
			Region of search			Hedgehog solution
	d (km)	β (km s^{-1})	d (km)	β (km s^{-1})	$\delta\beta_i$	β (km s^{-1})
a Greek-Albanian border	12.0	3.17	12.0	2.6 - 4.6	0.2	3.2 - 3.4
	15.0	3.44	15.0	3.0 - 5.0	0.2	3.2 - 3.6
	16.0	3.84	16.0	3.2 - 5.6	0.6	3.8 - 4.4
	17.0	4.27	17.0	3.4 - 5.8	0.6	4.0 - 4.6
		4.77		3.6 - 6.0	0.4	4.4 - 5.2
	$\chi 2$ = 0.170		a = 2, σ = 2			
b Ionian sea	12.0	3.04	12.0	2.6 - 4.6	0.2	3.0 - 3.0
	15.0	3.69	15.0	3.0 - 5.0	0.2	3.6 - 4.0
	16.0	3.99	16.0	3.2 - 5.6	0.2	3.6 - 4.8
		4.96	17.0	3.4 - 5.8	0.2	4.2 - 5.8
				3.6 - 6.0	0.2	4.2 - 5.6
	$\chi 2$ =0.735		a = 3, σ = 3			
c SW Peloponnese	12.0	2.88	12.0	2.6 - 4.6	0.4	3.0 - 3.0
	15.0	3.48	15.0	2.6 - 5.0	0.4	3.0 - 3.8
	16.0	3.44	16.0	2.6 - 5.6	0.4	3.0 - 4.6
	17.0	4.69	17.0	2.6 - 6.0	0.4	3.0 - 5.8
		4.56		2.6 - 6.0	0.4	3.0 - 5.4
	χ^2 = 0.367		a = 4, σ = 4			
d SW Crete	12.0	2.90	12.0	2.6 - 4.6	0.2	2.8 - 3.0
	15.0	3.54	15.0	3.0 - 5.4	0.4	3.4 - 3.4
	16.0	3.74	16.0	3.2 - 5.6	0.4	3.6 - 4.4
	17.0	4.56	17.0	3.4 - 5.8	0.4	3.8 - 5.8
		4.77		3.6 - 6.0	0.4	3.6 - 5.2
	χ^2 = 0.442		a = 3, σ = 3			
e Crete	18.0	3.17	18.0	2.0 - 4.6	0.2	3.0 - 3.6
	12.0	3.81	12.0	2.6 - 4.6	0.4	3.4 - 4.6
	30.0	4.19	15.0	3.2 - 5.2	0.4	3.6 - 4.8
		4.83	15.0	3.4 - 5.4	0.4	3.8 - 5.0
				3.6 - 6.0	0.4	4.4 - 5.6
	χ^2 = 1.971		a = 5, σ = 5			
f SE Crete	12.0	3.18	12.0	2.6 - 4.6	0.4	3.0 - 3.4
	15.0	3.68	15.0	2.8 - 5.2	0.4	3.2 - 4.0
	16.0	4.19	16.0	3.0 - 5.4	0.4	3.8 - 5.4
	17.0	5.04	17.0	3.4 - 5.8	0.4	4.2 - 5.4
		4.58		3.6 - 6.0	0.4	4.8 - 5.6
	χ^2 = 0.152		a = 4, σ = 4			
g Carpathos	10.0	3.02	10.0	2.6 - 4.6	0.5	3.1 - 3.1
	10.0	3.30	10.0	2.6 - 5.0	0.8	3.4 - 3.4
	11.0	4.19	11.0	2.6 - 5.4	0.7	3.3 - 4.7
	29.0	3.76	14.0	2.6 - 5.8	0.8	3.4 - 5.8
		4.17	15.0	2.6 - 5.8	0.8	3.4 - 5.0
				2.6 - 5.8	0.8	3.4 - 5.0
	χ^2 = 1.437		a = 4, σ = 4			
h Rhodes	20.0	3.19	10.0	2.6 - 4.6	0.4	3.0 - 3.4
	11.0	3.87	10.0	2.6 - 5.6	0.4	3.0 - 5.0
	29.0	4.32	11.0	2.6 - 5.6	0.4	3.0 - 4.6
		4.17	29.0	2.8 - 6.0	0.4	4.0 - 5.2
				2.8 - 6.0	0.4	3.6 - 4.4
	χ^2 = 1.918		a = 4, σ = 4			
i SW Turkey	16.0	3.26	16.0	2.6 - 4.6	0.5	3.1 - 3.6
	15.0	3.84	15.0	3.2 - 5.2	0.5	3.2 - 4.2
	11.0	3.72	11.0	3.4 - 5.4	0.4	3.8 - 5.4
	18.0	4.30	18.0	3.6 - 6.0	0.4	3.6 - 5.6
		4.59		3.6 - 6.0	0.6	4.2 - 5.4
	χ^2 = 0.238		a = 2, σ = 2			

Table 3. (*Continued.*)

	LINEAR INVERSION		HEDGEHOG INVERSION			
			Region of search			Hedgehog solution
	d (km)	β (km s^{-1})	d (km)	β (km s^{-1})	$\delta\beta_i$	β (km s^{-1})
j Central W. Turkey	7.0	3.08	7.0	2.6 - 4.6	0.4	3.0 - 3.0
	12.0	3.44	12.0	3.0 - 5.0	0.4	3.4 - 3.4
	12.0	4.34	12.0	3.0 - 5.4	0.4	3.4 - 4.6
	29.0	4.07	14.0	3.2 - 6.0	0.4	3.6 - 5.6
		4.40	15.0	3.2 - 6.0	0.4	3.2 - 5.6
				3.2 - 6.0	0.4	3.6 - 4.4
	χ^2 = 1.148		a = 3, σ = 3			
k Saros Gulf	7.0	2.87	7.0	2.6 - 4.6	0.4	2.6 - 3.0
	15.0	3.49	15.0	3.0 - 5.0	0.4	3.4 - 3.8
	15.0	4.86	15.0	3.2 - 5.6	0.4	4.4 - 5.2
	23.0	4.54	23.0	3.4 - 5.8	0.4	4.2 - 5.0
		4.81		3.6 - 6.0	0.4	4.0 - 5.2
	χ^2 = 6.627		a = 7, σ = 7			
l Chalkidiki	7.0	2.95	7.0	2.6 - 4.6	0.4	3.0 - 3.0
	12.0	3.45	12.0	2.6 - 5.0	0.4	3.4 - 3.4
	12.0	4.05	12.0	3.0 - 5.4	0.4	3.4 - 5.0
	29.0	4.62	14.0	3.2 - 5.6	0.6	3.8 - 5.0
		4.67	15.0	3.4 - 6.0	0.6	4.0 - 5.8
				3.6 - 6.0	0.6	3.6 - 5.4
	χ^2 = 0.299		a = 3, σ = 3			

and fourth layers to approaching and exceeding sub-Moho velocities.

The original Groups I and II apparent in the dispersion data are borne out in these inversions, with the Greek–Albanian border, Ionian sea, SW Peloponnese and SW Crete inversions showing similar characters at depth, usually a steady increase of velocity with depth reaching sub-Moho velocities in the layer below 43 km. Comparing the Ionian sea Hedgehog inversion with that for SE Crete, the latter shows a significant increase of velocity at shallower depth.

Carpathos and Rhodes (g–h of Figs 4 and 5)

The same starting model was used for both paths with only small modifications to the thickness and number of layers in the published reference model, in order to improve the solutions. The resulting inversions show (see g and h of Fig. 5) entry into an anomalous wedge of paths with evidence for a zone of low shear-wave velocity at depths well penetrated by the Rayleigh waves.

SW Turkey (i of Figs 4 and 5)

Although this path is close to those from Carpathos and Rhodes, a slightly different starting model improved the results. Fig. 5 again shows clear evidence of a zone of low shear-wave velocity along this path i; however, it is necessary to take into account the fact that the corresponding dispersion curve data are extracted from only two earthquakes and show the largest uncertainties around the critical maximum at the lower frequencies (Fig. 2i).

Central western Turkey (j of Figs 4 and 5)

This path has well-resolved dispersion data and their inversion confirms, again from a slightly different starting model, the azimuthal continuation of a low-velocity layer observed in this Group III of inversions.

Saros Gulf and Chalkidiki (k–l of Figs 4 and 5)

The starting model for the Saros Gulf path differs slightly to that used for Central western Turkey and Chalkidiki. The two paths from central western Turkey and the Saros Gulf, respectively, show similar characteristics in the linear inversion profiles which are brought out clearly in j and k of Fig. 5, despite some minor numerical differences. There is a gradual increase with depth of the shear-wave velocity from the first to the third layer inclusive, with a decrease to a low-velocity fourth layer followed by higher velocity at greater depth. However, the Saros Gulf path shows sub-Moho velocities within the 22–37 km third layer, implying that they commence at unusually shallow depth. There is a significant variation in velocity observed for both linear and Hedgehog inversions at the 22 km layer boundary depth. On the other hand, the Chalkidiki path l shows a more gradual increase of shear-wave velocity with depth; the increase of velocity in the third layer, which commences at 19 km, is clear but much less strong than that for the Saros Gulf path, and does not reach sub-Moho values until considerably greater depths. Unlike the paths from the adjacent Saros Gulf and the more distant central western Turkey, there is no low-velocity fourth layer zone along the Chalkidiki path.

The division of these inversions into Groups III and IV as for the observed dispersions curves is reasonable. The paths from Carpathos, Rhodes, SW Turkey, central western Turkey and the Saros Gulf generally show low-velocity layers in both the linear and Hedgehog inversions. The Saros Gulf path is particularly complicated, as seen in the observed dispersion curve (Fig. 2k). Group III represents the major anomalous wedge of paths with complex structures, which include low-velocity layers, edged by the transitional Group IV containing

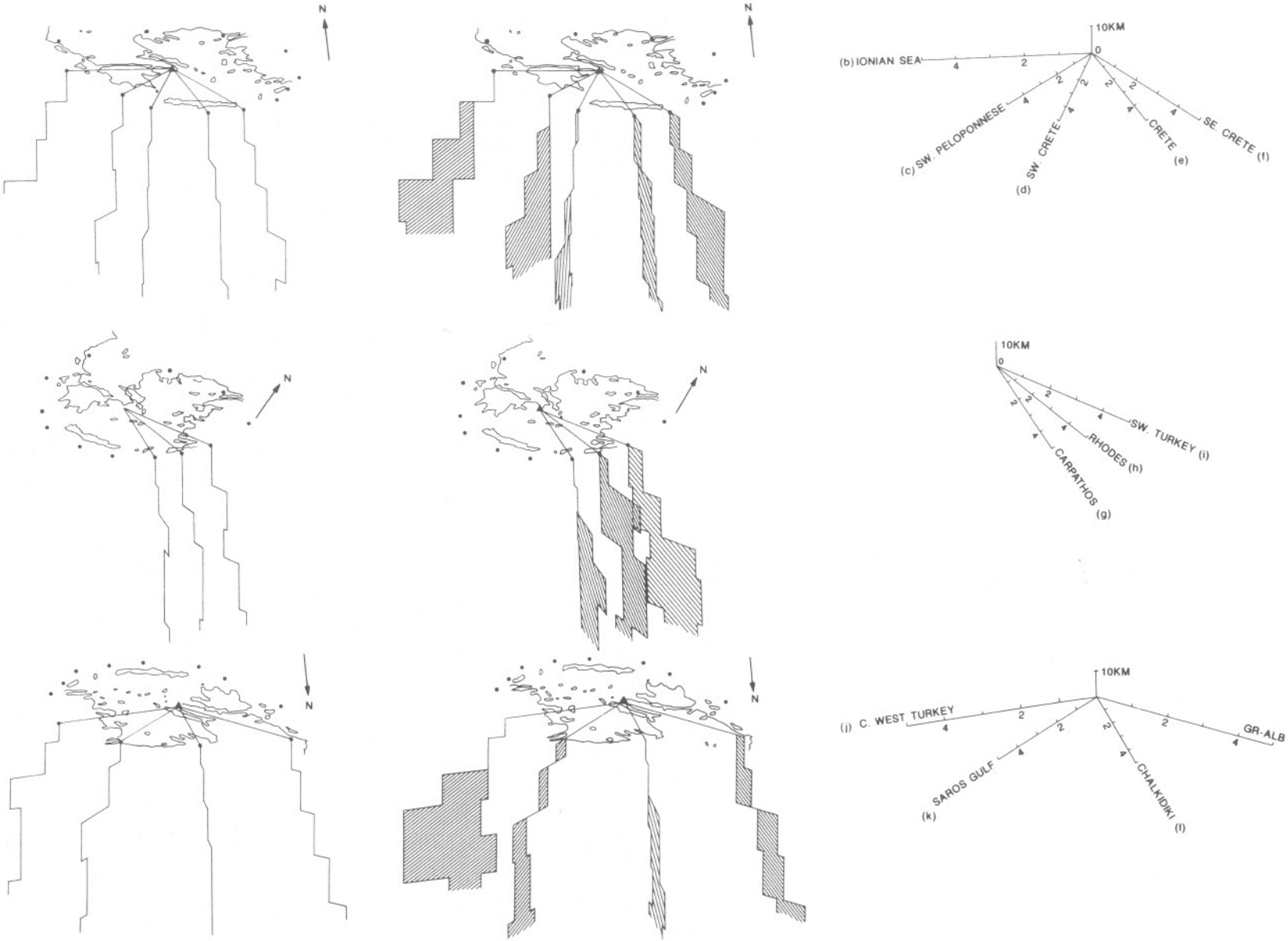

Figure 5. 3-D azimuthal perspectives of the shear-wave velocity–depth profiles below radial propagation paths a–l. The depth scale is constant. The shear-wave velocity scale (km s^{-1}) varies so that the length of the great-circle propagation path is proportional to the lowest velocity calculated for that path: shear-wave velocity scales specific to each propagation path are drawn (right column of the figure) at the corresponding azimuth to the velocity–depth profile. Line profiles represent linear inversions—left column—and shaded zones the regions of connected Hedgehog solutions—centre column (data from Table 3).

© 1996 RAS, *GJI* **125**, 679–695

the anomalous Saros Gulf path adjacent to the more typical Chalkidiki path, the latter path revealing a steady increase of shear-wave velocity with depth until sub-Moho velocities are reached.

5 DISCUSSION AND CONCLUSIONS

Generally the whole area is characterized by relatively low shear-wave velocities. The calculation and interpretation of the velocity in the upper layer also includes a well-known sedimentary layer (Payo 1967, 1969), with a thickness that varies between 3 and 8 km in western and southwestern Greece (Makris 1977, 1978; Panagiotopoulos 1984) and 1.5 km in eastern Greece (Panagiotopoulos 1984). The low shear-wave velocity of the first layer in the Saros Gulf and Chalkidiki paths could be explained partially by the thick sediments (reaching 6 km), which have been found from geophysical studies to fill the basins of the northern Aegean (Kiriakidis 1988), and partially by the seismotectonic regime of the area, described as an extensional field that causes the crust to thin. Papazachos & Comninakis (1978) proposed the existence of an old subduction zone in the northern Aegean and they assumed that extension takes place in the area.

The differences between the results for the paths crossing the south-western, southern and south-eastern Aegean may be explained by the subduction of not only one zone, but of various blocks, which affect the propagation of the waves by their different characteristics (e.g. angle of subduction and structure). Vanek *et al.* (1987) and Christova (1992) examined and proposed the existence of two different subduction zones, one western and one eastern, which do not join under Crete. A study of the mean station *P*-wave arrival-time residuals for local earthquakes shows a large contrast between two stations located on Crete (Ligdas *et al.* 1990). VAM (western Crete) has high positive residuals (indicating low velocities) relative to residuals close to zero (higher velocities) at NPS (eastern Crete). The paths from Carpathos, Rhodes and SW Turkey all traverse the Hellenic Volcanic Arc, where the heat flow is known to be high (e.g. Fytikas & Kolios 1979; Fytikas *et al.* 1989), and structure is expected to be anomalous here for this reason. There is also a growing view that there is a relative predominance of larger faults in this region (Vanek *et al.* 1987; Main & Burton 1989; Tsapanos, Galanopoulos & Burton 1994).

The possibility of resolving low-velocity layers is one of the advantages arising from the use of surface waves in structural studies. Although some of the earlier theoretical models used include low-velocity layers at depths of 100 km (Papazachos *et al.* 1967; Papazachos 1969), our data do not allow the structure to be studied in detail for depths below 70 or 80 km. However, there is clear evidence that low-velocity layers exist at depth along the Group III paths, and probably along those paths immediately adjacent to this group (from SE Crete and the Saros Gulf). The contoured velocity–depth panoramas of Fig. 6 have been drawn to consolidate the results in this context and to attempt to isolate low-velocity layers as low-velocity zones. The two panoramas in Fig. 6 are analogous to Fig. 3 in that they are azimuthally accurate, i.e. a–a represents 360° and the spans between propagation paths are proportional to the angles subtended at Athens. Fig. 6(a) summarizes the linear inversions and Fig. 6(b) the Hedgehog inversions. The spot values of shear-wave velocity in each vertical profile in Fig. 6(a) are the values of Table 3 rounded to one decimal place and entered into Fig. 6(a) at a depth corresponding to the middle of the layer concerned. The Hedgehog velocity values for each vertical profile in Fig. 6(b) are the middle of the Hedgehog solution range in each layer in Table 3 (and it should be noted that the resulting vertical profile of shear-wave velocities thus obtained is not necessarily an optimum Hedgehog solution); these are also entered at mid-layer depth. Shear-wave velocity values in the half-space are arbitrarily assigned a depth 10 km into the half-space, resulting typically in 70 km depth. The resulting grids of points have then been contoured at 0.25 km s^{-1} steps, producing seven contours from 3.0 to 4.5 km s^{-1}. In general the contoured azimuthal panoramas indicate that the depth at which the Moho surface appears is about 45 km for western Greece and in the range 20 to 35 km for the eastern and central Aegean, which is in agreement with results from previous investigations (Papazachos *et al.* 1966; Makris 1973, 1977, 1978; Panagiotopoulos 1984; Kiriakidis 1988). The most striking implications of Figs 6(a)–(b) can be summarized as follows.

(1) The overall patterns of results from linear and Hedgehog inversions are consistent and corroborative.

(2) The inversions for Group III paths, particularly from Carpathos, Rhodes and SW Turkey, inspected together resolve an extensive zone of relatively low shear-wave velocity (under 4.0 km s^{-1}) which is trapped and centred around 30 km depth and may extend from 20–40 km deep. The shear-wave velocity is typically about 3.8 km s^{-1} in this zone and is capped by a higher velocity of at least 4.0 km s^{-1} and a crustal lid of about 20 km thickness. This wedge of three paths subtends an angle of about 33° at Athens and traverses the Hellenic Volcanic Arc.

(3) There is slight evidence for anomalously low upper-mantle shear-wave velocities (under 4.25 km s^{-1} and around 4.1–4.2 km s^{-1}) along some paths at depths of 50–60 km, but these are at the physical limits of the lower-frequency Rayleigh-wave penetration depth and hence of useful resolution (bold dashed contours at greater depths in Figs 6a–b).

(4) The western wedge of paths, Chalkidiki anticlockwise round to SW Crete (1 and a–d in Fig. 6) all show deeply extending crustal velocities before sub-Moho velocities are encountered at about the 4.5 km s^{-1} contour.

The good quality and many years of continuity of operation of the National Observatory of Athens, which houses the long-period standard seismograph used in this study, has provided the opportunity to determine and examine the shear-wave velocity structure over the broader Aegean, centred on Athens. Some of the areas traversed by the Rayleigh waves need even more detailed inspection, particularly for paths traversing the Hellenic Volcanic Arc and the Saros Gulf, where anomalous structures are discernible. Records from other seismographs in the broader area and centred outside Athens could be used to seek this detailed improvement and perhaps extend the investigation to models of attenuation and damping of seismic energy (Delibasis 1982; Hashida *et al.* 1988) in the broader Aegean.

ACKNOWLEDGMENTS

We are grateful to an anonymous referee for comments that substantially improved the draft paper. ISK thanks the School of Environmental Sciences, University of East Anglia for

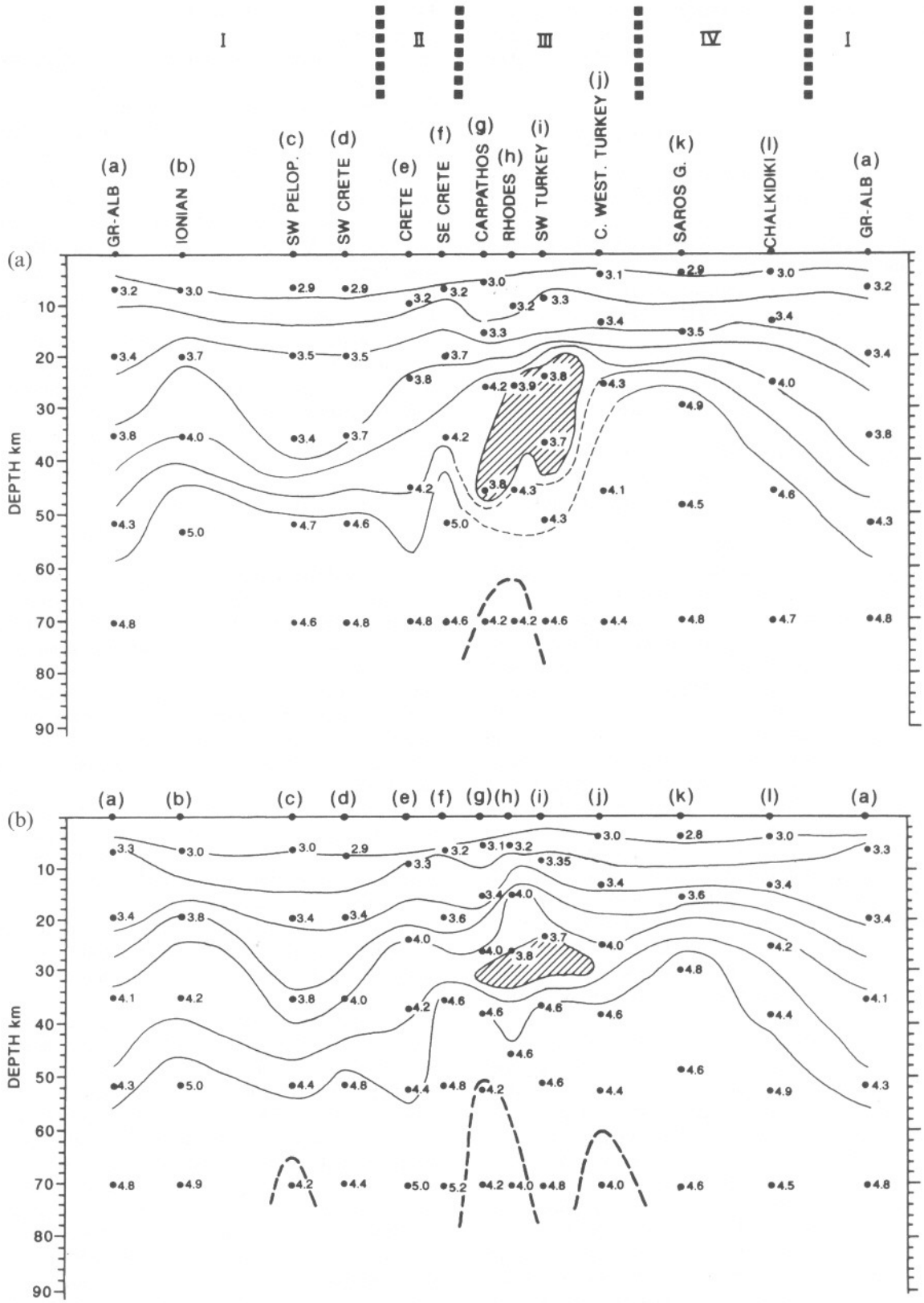

Figure 6. Contoured shear-wave velocity–depth panoramas of the broader Aegean. Spot shear-wave velocity values in (a) from linear inversions and (b) from Hedgehog solutions are taken from Table 3 and entered at the mid-depth of each layer in each individual velocity–depth profile a–l (see text for further explanation). The resulting grids of shear-wave velocities are contoured in 0.25 km s^{-1} steps from 3.0 km s^{-1} near the surface to 4.5 km s^{-1} (approximately sub-Moho velocities) at depth. The hatched area is a trapped low-velocity zone (under 4.0 km s^{-1}) resolved by the wedge of paths from Carpathos, Rhodes and SW Turkey which traverse the Hellenic Volcanic Arc. The bold dashed contours indicate slight evidence for anomalously low upper-mantle shear-wave velocities (around 4.1–4.2 km s^{-1}). The length a–a represents 360° and spacings between radial propagation paths are proportional to the angle subtended at Athens.

funding enabling completion of this paper in Norwich, and PWB acknowledges NERC Grant GR9/1005A and NATO Collaborative Research Grant 9407180, the travel elements of which aided this work.

REFERENCES

Backus, G. & Gilbert, F., 1967. Numerical application of a formalism for the geophysical inverse problems, *Geophys. J. R. astr. Soc.*, **13,** 247–276.

Backus, G. & Gilbert, F., 1968. The resolving power of gross Earth data, *Geophys. J. R. astr. Soc.*, **16,** 169–205.

Backus, G. & Gilbert, F., 1970. Uniqueness in the inversion of inaccurate gross earth data, *Phil. Trans. R. Soc. Lond.*, A, **266,** 123–192.

Burton, P.W. & Blamey, C., 1972. A computer program to determine the spectrum and a dispersion characteristic of a transient signal, *UKAEA AWRE, Report No 0–48/72,* HMSO.

Calcagnile, G., D'Ingeo, F., Farrugia, P. & Panza, G.F., 1982. The lithosphere in the central-eastern Mediterranean area, *Pure appl. Geophys.*, **120,** 389–406.

Christova, C., 1992. Seismicity depth pattern, seismic energy and b-value depth variation in the Hellenic Wadati–Benioff zone, *Phys. Earth planet. Inter.*, **72,** 38–48.

Christova, C. & Nikolova, S.B., 1993. The Aegean region: deep structures and seismological properties, *Geophys. J. Int.*, **115,** 635–653.

Cooley, J.W. & Tukey, J.W., 1965. An algorithm for the machine calculation of complex Fourier series, *Mathematics of Computation,* **19,** 297–301.

Delibasis, N.D., 1982. Seismic wave attenuation in the upper mantle beneath the Aegean region, *Pure appl. Geophys.*, **120,** 820–839.

Dziewonski, A., Bloch, S. & Landisman, M., 1969. A technique for the analysis of transient seismic signals, *Bull. seism. Soc. Am.*, **59,** 427–444.

Espinosa, A.F., Sutton, G.H. & Miller, H.J., 1965. *A transient technique for seismograph calibration—Manual and standard set of theoretical transient responses,* Geophys. Lab., Inst. Sci. Techn., Univ. of Michigan.

Ezen, U., 1988. An interference phenomenon in Rayleigh wave trains associated with the earthquakes in and around the Aegean Sea, *Bull. Int. Instit. Seism. Earthq. Engin.*, **20,** 33–62.

Ezen, U., 1991a. Crustal structure of western Turkey from Rayleigh wave dispersion, *Bull. Int. Instit. Seism. Earthq. Engin.*, **25,** 1–21.

Ezen, U., 1991b. Surface wave dispersion and upper crustal structure along N–S direction in western Turkey from Burdur earthquake of 12 May 1971, *Bull. Int. Instit. Seism. Earthq. Engin.*, **25,** 39–59.

Fytikas, M.D. & Kolios, N.P., 1979. Preliminary heat-flow map of Greece, in *Terrestrial Heat Flow in Europe,* Cermak, V. & Rybach, L., Springer-Verlag.

Fytikas, M.D., Garnish, J.D., Hutton, V.R.S., Staroste, E. & Wohlenberg, J., 1989. An integrated model for the geothermal field of Milos from geophysical experiments, *Geothermics,* **18,** 611–621.

Hashida, T., Stavrakakis, G & Shimazaki, K., 1988. Three-dimensional seismic attenuation structure beneath the Aegean region and its tectonic implications, *Tectonophysics,* **145,** 43–54.

Hatzfeld, D., Besnard, K., Makropoulos, K. & Hatzidimitriou, P., 1993. Microearthquake seismicity and fault-plane solutions in the southern Aegean and its geodynamic implications, *Geophys. J. Int.*, **115,** 799–818.

Kalogeras, I.S., Drakopoulos, J.K. & Burton, P.W., 1993. Dispersion curves for the path Dodecanese islands–ATH as inferred from the analysis of the Rayleigh wave records, in *Proc. 6th Congress of the Geol. Soc. Greece, Bull. geol. Soc. Greece*, **28**, 213–222 (in Greek).

Keilis-Borok, V.I. & Yanovskaja, T.B., 1967. Inverse problems of seismology (structural review), *Geophys. J. R. astr. Soc.*, **13,** 223–234.

Keller, G.R., Smith, R.B., Braile, L.W., Heaney, R. & Shurbet, D.H., 1976. Upper crustal structure of the eastern Basin and Range, Northern Colorado Plateau and Middle Rocky Mountains from Rayleigh wave dispersion, *Bull. seism. Soc. Am.*, **66,** 869–876.

Kiriakidis, L.G., 1988. The crustal structure in northern Greece, in *Proc. 1st Symp, The new evolutions on Seismology and Geophysics in Greece,* 409–436, Geophysical Laboratory of the Aristotelian University of Thessaloniki (in Greek).

Knopoff, L., 1972. Observation and inversion of surface wave dispersion, in *The upper mantle, Tectonophysics,* ed. Ritsema, A.R., **13 (1-4),** 497–519.

Le Pichon, X. & Angelier, J., 1979. The Hellenic arc and trench system: A key to the Neotectonic evolution of the eastern Mediterranean region, *Tectonophysics,* **60,** 1–42.

Ligdas, C.N., Main, I.G. & Adams, R.D., 1990. 3-D structure of the lithosphere in the Aegean region, *Geophys. J. Int.*, **102,** 219–229.

Main, I.G. & Burton, P.W., 1989. Seismotectonics and the earthquake frequency–magnitude distribution in the Aegean area, *Geophys. J. R. astr. Soc.*, **98,** 575–586.

Makris, J., 1973. Some geophysical aspects of the evolution of the Hellenides, *Bull. Geol. Soc. Greece,* **10,** 206–213.

Makris, J., 1975. Crustal structure of the Aegean Sea and the Hellenides obtained from geophysical surveys, *J. geophys. Res.*, **41,** 441–443.

Makris, J., 1977. Geophysical investigations of the Hellenides, *Geophys. Einzelschr., Hamburger,* **34.**

Makris, J., 1978. The crust and upper mantle of the Aegean region from deep seismic soundings, *Tectonophysics,* **46,** 269–284.

Makropoulos, K.C. & Burton, P.W., 1984. Greek tectonics and seismicity, *Tectonophysics,* **106,** 275–304.

Panagiotopoulos, D.G., 1984. Travel time curves and crustal structure in the southern Balkan region, *PhD thesis,* University of Thessaloniki, Greece (in Greek).

Papazachos, B.C., 1969. Phase velocities of Rayleigh waves in Southeastern Europe and Eastern Mediterranean Sea, *Pure appl. Geophys.*, **75,** 47–55.

Papazachos, B.C. & Comninakis, P.E., 1978. Geotectonic significance of the deep seismic zones in the Aegean area, in *2nd Inter. Sci. Conf. Thera and the Aegean World,* pp. 101–109, eds Doumas, C. & Puchelt, H.C., Bishopsgate, London.

Papazachos, B.C., Comninakis, P.E. & Drakopoulos, J.K., 1966. Preliminary results of an investigation of crustal structure in southeastern Europe, *Bull. seism. Soc. Am.*, **56,** 1241–1263.

Papazachos, B., Polatou, M. & Mandalos, N., 1967. Dispersion of surface waves recorded in Athens, *Pure appl. Geophys.*, **67,** 95–106.

Payo, G., 1967. Crustal structure of the Mediterranean Sea by surface waves, Part I: Group velocity, *Bull. seism. Soc. Am.*, **57,** 151–172.

Payo, G., 1969. Crustal structure of the Mediterranean Sea, Part II: Phase velocity and travel times, *Bull. seism. Soc. Am.*, **59,** 23–42.

Schwab, F.A. & Knopoff, L., 1972. Fast surface wave and free mode computations, in *Methods in computational physics, Vol. II. Seismology: Surface waves and earth oscillations,* pp. 87–180, ed. Bolt, B.A., Academic Press, New York, NY.

Spakman, W., Wortel, M.J.R. & Vlaar, N.G., 1988. The Hellenic subduction zone: a tomographic image and its geodynamic implications, *Geophys. Res. Lett.*, **15,** 60–63.

Tsapanos, T., Galanopoulos, D. & Burton, P.W., 1994. Seismicity in the Hellenic Volcanic Arc: relation between seismic parameters and the geophysical fields in the region, *Geophys. J. Int.*, **117,** 677–694.

Valus, V.P., 1968. *Vichislitelnaya Seismologiya,* **4,** 1.

Vanek, J., Hanus, V., Christova, C. & Simeonova, S., 1987. Morphology of the Wadati–Benioff zone in the Hellenic Arc, *J. Geodyn.*, **8,** 79–93.

Wiggins, R.A., 1972. The general linear inverse problem: Implications of surface waves and free oscillations for earth structure, *Rev. Geophys. Space Phys.*, **10,** 251–285.